Energy & Environmental Science

RSC Publishing

PAPER

View Article Online
View Journal | View Issue

Capture and electrochemical conversion of CO_2 to value-added carbon and oxygen by molten salt electrolysis†

Cite this: *Energy Environ. Sci.*, 2013, **6**, 1538

Huayi Yin,[a] Xuhui Mao,[a] Diyong Tang,[a] Wei Xiao,[a] Luru Xing,[a] Hua Zhu,[a] Dihua Wang*[a] and Donald R. Sadoway[b]

A molten salt electrochemical system comprising a eutectic mixture of Li–Na–K carbonates, a Ni cathode, and a SnO_2 inert anode is proposed for the capture and electrochemical conversion of CO_2. It is demonstrated that CO_2 can be effectively captured by molten carbonates, and subsequently electrochemically split into amorphous carbon on the cathode, and oxygen gas at the anode. The carbon materials generated at the cathode exhibit high BET surface areas of more than 400 $m^2\ g^{-1}$ and as such, represent value-added products for a variety of applications such as energy storage and pollutant adsorption. In the carbonate eutectic (500 °C), the presence of Li_2CO_3 is shown to be required for the deposition of carbon from the melt, wherein O^{2-} or Li_2O serves as the intermediate for CO_2 capture and electrochemical conversion. SnO_2 proved to be an effective anode for the electrochemical evolution of oxygen. Electrochemical reactions were found to proceed at relatively high current efficiencies, even though the current densities exceed 50 mA cm^{-2}. The intrinsic nature of alkaline oxides for CO_2 capture, the conversion of CO_2 to value-added products, and the ability to drive the process with renewable energy sources such as solar power, enables the technology to be engineered for high flux capture and utilization of CO_2.

Received 19th November 2012
Accepted 25th February 2013

DOI: 10.1039/c3ee24132g

www.rsc.org/ees

Broader context

Due to the link between CO_2 accumulation in the atmosphere and global warming, there is a worldwide growing awareness that the anthropogenic CO_2 emissions should be reduced. The electrochemical process, which is amenable to combine with renewable energy source like solar power, is one of the best promising routes that can simultaneously address the capture and utilization of CO_2 gas. In the Li–Na–K eutectic carbonate melts, we designed and assembled a novel electrolytic system consisting of an affordable nickel metal cathode and a SnO_2 inert anode. The nickel cathode can reduce the captured CO_2 (in the forms of carbonate anions) to capacitive carbon materials for energy storage and pollutants absorption, which exhibited high BET surface areas of more than 400 $m^2\ g^{-1}$. The SnO_2 proved to be a chemically stable anode for the electrochemical evolution of oxygen in this molten alkaline carbonate system. The overall system working at 500 °C can exclusively produce carbon and oxygen at reasonable current efficiencies. The ultimate goal of the research is to engineer the current process for high flux capture and utilization of CO_2 at a large scale, and solar power can be the direct energy input for the process.

Introduction

Restraining the continuous increase of CO_2 concentration in the atmosphere has attracted significant attention due to the great concern of global climate change.[1–3] CO_2 capture and storage (CCS) as well as utilization of CO_2 have attracted the attention of researchers hoping to achieve a meaningful reduction in CO_2 emissions in the near-term.[4] As the most oxidized state of carbon, CO_2 is usually the ultimate product of most energy releasing processes. Pure CO_2 is an ideal C^1 feedstock for many industrial processes, such as the productions of urea, salicylic acid, carbamates and inorganic compounds.[5–7] Therefore, many attempts have been carried out to capture CO_2 from atmospheric or effluent gases, and recycle the captured CO_2 into a raw material for industrial processes.[8] On the other hand, reducing CO_2, which mimics the photosynthesis of plants, is another pathway to utilize the captured CO_2. At present, the technological options that are commonly studied for transforming CO_2 include:[9] (1) chemical transformation of CO_2 to hydrogenated

[a]*School of Resource and Environmental Science, Wuhan University, Wuhan 430072, China. E-mail: wangdh@whu.edu.cn; Fax: +86-27-6877-5799; Tel: +86-27-6877-4216*

[b]*Department of Materials Science and Engineering, Massachusetts Institute of Technology, Cambridge, MA 02139, USA. E-mail: dsadoway@mit.edu; Tel: +1-617-253-3487*

† Electronic supplementary information (ESI) available: Thermodynamics data and dissociation potential of typical reactions, BET surface area and TEM images of the obtained carbon powder, element composition of the prepared carbon by XRF measurement, CVs of the Ni electrode in the melts, relationship between equilibrium constant and temperature, CVs and EIS of the carbon film electrode in 1 M H_2SO_4 solution, photos of different anodes applied in the melt, and experimental information. See DOI: 10.1039/c3ee24132g

materials (hydrocarbons, MeOH, EtOH, *etc.*), (2) photochemical transformation to CO, HCO_2H, CH_4, (3) electrochemical/photoelectrochemical transformation to CO, HCO_2H, MeOH in ionic liquids, (4) biological transformation to EtOH, sugar, CH_3CO_2H, and (5) reforming CO_2 to generate CO and H_2.

Due to the chemical stability of CO_2, energy in the form of light, electricity, or high-energy starting materials, along with catalysts are needed to convert CO_2 at an acceptable transformation rate.[6,8,10] Electrochemical reactions take place at the interface between the electrode and the electrolyte, where electrons directly serve as strong redox reagents for the transformation of target compounds, and therefore refractory substances like CO_2 can be directly reduced under mild conditions. The electrochemical reduction of CO_2 was firstly investigated in aqueous solution, however, due to low solubility of the gas in aqueous solution and the proximity of the electroreduction potentials of CO_2 and water decomposition, electrochemical transformation of CO_2 in aqueous solution is sluggish and impractical.[11] More recently, electrochemical reduction of CO_2 was investigated in room temperature ionic liquids (RTILs) owing to their wide electrochemical window and high solubility of CO_2 in them.[12,13] Although the product yield was reportedly higher than that in aqueous solution,[13] the current high cost of RTILs remains an impediment to their widespread adoption in certain commercial applications.[12,14,15] Carbonate melts are low cost electrolytes with high ionic conductivity and low vapor pressure and are used as alternatives for electrochemical processing of CO_2. Ito and Kawamura reported that a carbon film was electrochemically deposited on an aluminum electrode in LiCl–KCl–K_2CO_3 melts when CO_2 was fed into the electrolytic system.[16] Groult *et al.* reported synthesis of a nanostructured carbon material by electroreduction in fused alkaline carbonates.[17–19] Recently, Kaplan *et al.* developed an electrochemical reaction of converting CO_2 to CO with the thermodynamic efficiency exceeding 85% in molten Li_2CO_3 at 850–900 °C using a titanium cathode and a graphite anode.[20] The reaction current density at the temperature is ~100 mA cm^{-2},[20] much higher than that in aqueous solution.[21] Licht *et al.* reported a solar thermal carbon capture process consisting of a Li_2CO_3 molten electrolyte, a nickel cathode and a Pt anode, CO_2 was electrochemically reduced to CO and C at 750–950 °C.[22] It was more recently reported that mild steel[23] or titanium[24] can be electro-carburized using CO_2 feedstock in molten carbonate salts to form an effective case hardened surface. These studies demonstrated that the electrochemical reduction of carbonate is greatly impacted by the reaction conditions, such as temperature, cell voltage and melt composition, for example, the higher the temperature, the more probable the production of CO.[20,22]

In the present study, we propose a novel molten electrochemical process for the capture and utilization of CO_2. CO_2 from effluent gases is captured in the molten Na_2CO_3–K_2CO_3–Li_2CO_3 eutectic at 500 °C, and electrochemically split into carbon and oxygen between a nickel (Ni) plate cathode and a SnO_2 inert anode. Owing to the unique processing conditions in molten salts, the obtained carbon features huge specific surface area, being advantageous for its use in supercapacitors as well as carbonaceous adsorbents. The oxygen from the CO_2 splitting reactions can be used as the combustion gas for oxyfuel processes, which decreases the generation of CO and facilitates the recycling of CO_2. Unlike previously reported CCS processes, the process proposed herein not only effectively captures CO_2 from influent, but also converts it into valuable products, namely oxygen gas and capacitive/absorptive carbon. Considering that an electrochemical process can be easily driven with renewable energy sources such as solar and wind, the present method can be exploited as a large-scale molten salt CO_2 capture and electrochemical transformation (MSCC-ET) process, as shown in Scheme 1. The objective of this study is to explore the feasibility of the MSCC-ET process, and to evaluate the validity of anodes and the current/energy efficiencies of the electrochemical processes in Na_2CO_3–K_2CO_3–Li_2CO_3 eutectic molten salts.

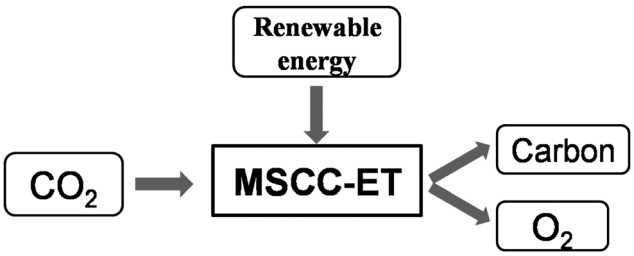

Scheme 1 Schematic illustration of the Molten Salt CO_2 Capture and Electrochemical Transformation (MSCC-ET) process.

Experimental

Anhydrous Li_2CO_3, Na_2CO_3, and K_2CO_3 were of analytical purity from Sinopharm Chemical Reagent Co., Ltd. Nickel, copper, platinum and iridium wires used as working electrodes (1 mm diameter) for cyclic voltammetry (CV) measurements were of more than 99.9% purity. SnO_2 anodes (STANNEX E) were provided by Dyson Thermal Technologies. A $Ni_{10}Cu_{11}Fe$ anode was prepared in the authors' lab, and the information regarding the preparation can be found in a previous report.[25]

The electrolysis cell consisted of an alumina crucible filled with 500 g of Li_2CO_3, Na_2CO_3 and K_2CO_3 (43.5 : 31.5 : 25 mol%). The crucible was sealed in a steel reactor heated by a tube furnace. Before electrochemical measurements, the temperature of the furnace was kept at 150 °C for 12 hours in a vacuum to remove moisture of the carbonates. Afterwards the temperature of the steel reactor was slowly raised to 500 °C in the CO_2 atmosphere to melt the salts. In order to remove impurities and residual water, pre-electrolysis was conducted using a SnO_2 anode and a nickel sheet cathode under a constant cell voltage of 1.5 V for 2 hours. CO_2 was continuously bubbled into the melt through an alumina tube during electrochemical tests and electrolysis experiments. CV measurements were performed on an electrochemical workstation (CHI-1140, CH Instrument Co. Ltd., USA) using a three-electrode configuration. A silver wire was used as a quasi-reference electrode in the melts. Constant cell voltage electrolysis was carried out in the molten Li_2CO_3–Na_2CO_3–K_2CO_3 eutectic (500 °C) using a computer-controlled

power source (Shenzhen Neware Electronic Co. Ltd., China). Unless specifically mentioned, a Ni sheet and a SnO_2 rod served as a cathode and an anode, respectively, for constant cell voltage electrolysis. The effluent gas from the reactor was monitored by a gas chromatograph equipped with a thermal conductivity detector and a SE-30 column (GC9800, Shanghai Kechuang Chromatograph Instruments Co. Ltd., China). Detailed information regarding the GC analytical procedure can be found in the ESI.† After electrolysis, the cathode was lifted out of the melt and cooled down in the headspace of the reactor. Thereafter, the cathode was taken out and rinsed with 1 M HCl to remove the adherent frozen electrolyte and was dried in a vacuum oven at 80 °C for 12 hours.

The carbon products were characterized by cyclic voltammetry (CV) as well as charge–discharge tests in 1 M H_2SO_4 aqueous solution using a CHI 1140 electrochemical workstation. A platinum plate and a saturated calomel electrode (SCE) served as counter and reference electrodes, respectively. The working electrode with the thickness of approximately 100 μm was prepared by mixing and kneading the as-prepared carbon powder (80 wt%) with acetylene black (10 wt%) and a Teflon binder (10 wt %) and then pressing on a titanium mesh. The obtained carbon was also evaluated by Cr(VI) adsorption experiments carried out at 20 °C. 50 mg carbon powders were added into a conical flask prefilled with 50 mL of 50 mg L^{-1} dichromate aqueous solution, and the flask was left on a thermostatic shaker (120 rpm) for 4 hours. Afterwards, the solution was centrifuged and the dichromate concentration of the supernatant was examined using a photospectrometer (UV-9100, Ruili analytical company, Beijing) at 545 nm wavelength.[26] The absorption capacity of the carbon powder was calculated by the difference of dichromate concentrations before and after experiments.

The obtained products on the cathode were characterized by X-ray diffraction spectroscopy (XRD, Shimadzu X-ray 6000 with Cu Kα1 radiation at $\lambda = 1.5405$ Å), scanning electron microscopy (SEM, FEI Sirion field emission), transmission electron microscopy (TEM, JEM2010-HT) and Brunauer–Emmett–Teller (BET, Gemini V Analyzer) analysis, and confocal Raman microspectroscopy (Renishaw, RM-1000) with an excitation at 514.5 nm. The elemental composition of the carbon powder was measured on a S4 Pioneer X-ray fluorescence spectrometer (XRF, Brucker AXS) by a standardless analysis method. The procedure of the calcination experiment for carbon powders is provided in the ESI.†

Results and discussion

Cathodic production of carbon

Fig. 1 shows the cyclic voltammograms of the Ni electrode in the Li_2CO_3–K_2CO_3–Na_2CO_3 eutectic molten salt at 500 °C. When the potential scan range is between −0.6 V and −1.8 V, no redox peak is observed in the forward or reverse scan (red curve in Fig. 1a). When the cathodic scan reaches −2.4 V, two reduction peaks (c1 and c2) and their corresponding oxidation peaks (a1 and a2) can be observed. The reduction peak c2 apparently represents the limit of the supporting electrolyte and indicates

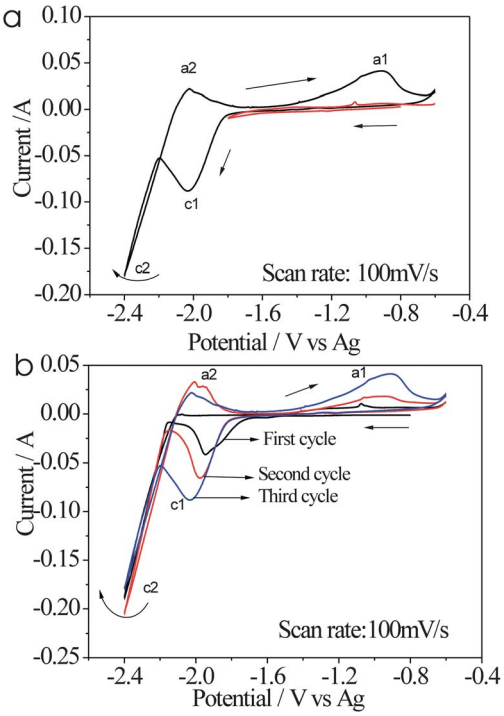

Fig. 1 Cyclic voltammograms recorded from a Ni electrode in the molten Li_2CO_3–Na_2CO_3–K_2CO_3 at 500 °C in the CO_2 atmosphere (a) in different potential ranges and (b) under consecutive cycling.

the deposition of alkaline metals. The potential of the peak c1 is ~0.4 V positive of the deposition potential of alkaline metals (c2), suggesting the occurrence of reduction of CO_3^{2-} and deposition of carbon.[17] The oxidation peaks a1 and a2 clearly result from the electrochemical dissolution of the deposited alkaline metals and carbon, which can be verified by the CVs of successive scans (Fig. 1b). As can be observed, with the increase in scan cycles, the reduction currents at c1 and the anodic currents at a1 increase correspondingly, showing similar trends as a function of scan cycles. This observation can be explained by the formation of the conductive carbon on the Ni cathode and the growth of the surface area of the working electrode, resulting in continuous rising of redox currents. The CV results herein are consistent with those in the literature. Groult *et al.* reported the CV of a vitreous carbon electrode in Li–Na–K carbonate melts at 700 °C, and a similar reduction peak of CO_3^{2-} and the corresponding oxidation peak of carbon were observed.[17] Furthermore, the reduction of CO_3^{2-} produces carbon instead of CO when the working temperature of Li_2CO_3 melts is lower than 850 °C.[22]

In the eutectic melts of the present study, the carbonate ions may be reduced to carbon according to the following processes:

$$CO_3^{2-} + 4e^- = C + 3O^{2-} \quad (1a)$$

$$C_{(n+1)}O_{(2n+3)}^{2-} + 4e^- = C + nCO_3^{2-} + 3O^{2-} \quad (1b)$$

When the CO_2 from the effluent gas is bubbled into the eutectic melts, reactions forming carbonates (*e.g.* CO_3^{2-}, and $C_{(n+1)}O_{(2n+3)}^{2-}$) occur[27,28] and CO_2 is captured:

$$O^{2-} + CO_2\,(g) = CO_3^{2-} \quad (2)$$

$$CO_3^{2-} + CO_2\,(g) = C_2O_5^{2-} \quad (3)$$

$$CO_3^{2-} + nCO_2\,(g) = C_{(n+1)}O_{(2n+3)}^{2-} \quad (4)$$

In order to make the whole process work effectively, a eutectic mixture of Li–Na–K carbonates is adopted for testing the feasibility of MSCC-ET in this study. As we know, a eutectic mixture is advantageous for lowering the working temperature of melts, thus enabling less energy consumption and less caustic condition for electrolysis. In addition, previous studies showed that lower reaction temperature favored the production of carbon, instead of CO, on the cathode.[22] However, the role of individual carbonates for the electrochemical process is quite different. Among the three alkali carbonates, Li_2CO_3 is essentially required for the deposition of carbon from electrochemical reduction of molten alkali carbonates.[19] This view point was further confirmed by the CV measurement conducted in this laboratory. In Na_2CO_3–K_2CO_3 melts (see Fig. S1 in the ESI†) at 750 °C, no carbon reduction peak was found in the absence of Li_2CO_3. In Table S1 of the ESI,† the Gibbs energy (ΔG) and reaction potential (ΔE) for the dissolution of alkali metal carbonate into carbon and alkali oxide (se1 to se3, in Table S1 of the ESI†), into alkali metal, carbon and oxygen (se4 to se6, in Table S1 of the ESI†) were calculated using HSC-5.0 software. The calculated results clearly show that the electrochemical reduction of Li_2CO_3 into lithium metal needs high decomposition potential, while the dissolution of Li_2CO_3 into lithium oxide and carbon is much more favored in comparison with Na_2CO_3 and K_2CO_3. In contrast, if O_2 evolution is used as the reference anodic reaction, the potential of carbon generation in Na_2CO_3 or K_2CO_3 melts is even more negative than the deposition potential of the alkali metal. Therefore, a separate reduction current peak associated with carbon generation was not observed in the Na_2CO_3–K_2CO_3 binary melts. Moreover, according to our Gibbs energy calculations (se11 and se12, in Table S1 of the ESI†), lithium oxide is the most stable alkali metal oxide that exists in the eutectic melts. This means that when alkali carbonates are electrochemically decomposed, Li_2O instead of Na_2O or K_2O, will serve as intermediate for the capture of CO_2, allowing the continuous operation of the MCSS-ET process.

Li_2O in the Li_2CO_3 melt is proven to be capable of absorbing CO_2 in the temperature range of 750–950 °C.[20,22,29] At lower temperatures, the thermodynamic data regarding the interaction of Li_2O and the eutectic melts are not available for a precise calculation of the equilibrium constant (K) of reaction se13, however, a rough estimation using standard ΔG can be conducted. An increase in equilibrium constant with the decrease of temperature can be observed in Fig. S2 in the ESI,† indicating that Li_2O has stronger affinity for CO_2 at 500 °C in comparison with that of 750–950 °C (equilibrium constant of reaction se13 is 9.62×10^6 at 500 °C). Therefore, an efficient reaction between Li_2O and CO_2 is expected in this eutectic system. Actually, in the constant-voltage electrolysis experiments, the alkalinity of the eutectic electrolytes after several hours of operation did not show appreciable change when CO_2 gas was continuously fed, suggesting that Li_2O did not accumulate in the electrolyte, and only served as the intermediate for CO_2 transformation. Besides, it should be pointed out that CO_2 can dissolve into the Li–Na–K carbonate eutectic through reaction (3).[27,28]

Electrolysis experiments were further conducted for investigating the carbon materials deposited on the Ni cathode. In Fig. 2a, the Ni cathode after 5 hours of electrolysis under a constant cell voltage of 4.0 V is shown. As can be seen, a thick layer of porous carbon formed on the Ni sheet cathode, suggesting the newly formed carbon can serve as a conductive substrate for successive deposition. The XRD spectra of the carbon powders obtained at different cell voltages indicate that they are all amorphous carbon (Fig. 2b). The Raman spectra in Fig. 2c also show the characteristic peaks of active carbon materials, G band at 1580 cm^{-1} and D band at 1370 cm^{-1}.[30] In Fig. 2d–i, the carbon materials prepared at different cell voltages exhibit similar microstructures except for the one obtained at 2.8 V. The carbon obtained at 2.8 V has a flake-like structure, while the others look like aggregates of carbon nanoparticles. The observation was further evidenced by the TEM images (Fig. S3†): the product obtained at 2.8 V is a carbon film, while the product at 4.0 V is flocculent carbon. XRF measurement showed that the carbon powder prepared at 4.5 V and 450 °C contained 0.89 wt% impurity (see Table S3 in the ESI†), and the residual ash after 2 hours of calcination in air at 800 °C was less than 1%.

The electrolytic fine carbon powders are electronically conductive and they exhibit high BET surface areas ranging from 414 to 616 $m^2\ g^{-1}$ as shown in Table S2.† Therefore, the carbon was further characterized in the manner fitting for capacitive and adsorptive materials. Both the CVs and EIS spectrum in Fig. S4† indicate that the prepared carbon featured typical capacitive behaviors in 1 M H_2SO_4 solution.[31] Fig. 3a presents the constant current charge–discharge profiles of the carbon from which the specific capacitances are calculated to

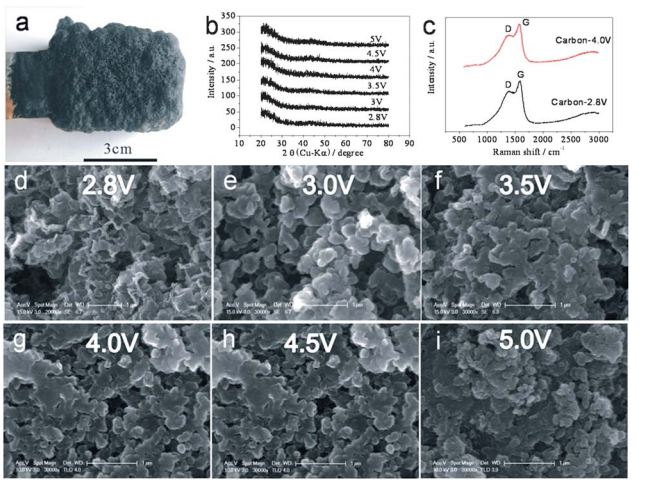

Fig. 2 (a) Digital photo of a Ni cathode after 5 hours of electrolysis under 4.0 V cell voltage; (b) XRD patterns of the carbon deposited at the indicated cell voltages; (c) Raman spectra of the carbon obtained at 2.8 V and 4.0 V and (d–i) SEM images of the carbon obtained at the indicated conditions.

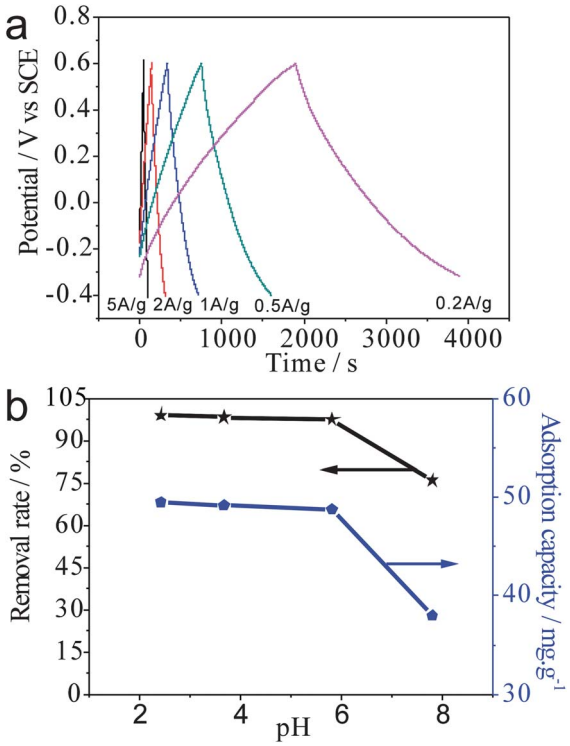

Fig. 3 (a) Charge–discharge curves of the carbon material obtained at 4.0 V cell voltage in 1 M H_2SO_4 aqueous solution and (b) adsorption capacity and the removal rate of Cr(VI) by the carbon obtained at 4.0 V, the initial concentration of Cr(VI) was 50 mg L^{-1}.

be 270, 330, 376 and 400 F g^{-1} at current densities of 5, 2, 1, 0.5 and 0.2 A g^{-1}, respectively. The capacitive property of the prepared carbon powders is superior to that of the reported commercial active carbons,[32] being advantageous for its use as a supercapacitor material. Furthermore, the adsorption capacity of the carbon for Cr(VI) was evaluated at different values of pH. As presented in Fig. 3b, 99% removal rate and the highest adsorption capacity of 49.5 mg g^{-1} are achieved at pH 2.4, at which the $HCrO_4^-$ is the major Cr(VI) species that favors adsorption.[33] Under the same experimental conditions, the deposited carbon in this study presented absorption capacity similar to commercial active carbon absorbents.[34] To summarize, the cathodically generated carbon exhibits good capacitive performance and comparable adsorption capacity for Cr(VI) and thus demonstrates itself to be a value-added product of the MSCC-ET process.

Anodic production of O_2

In the Li–Na–K carbonate eutectic melts, O^{2-} or CO_3^{2-} are the anions that can be oxidized to oxygen gas:

$$O^{2-} - 2e^- = 0.5O_2\ (g) \quad (5)$$

$$C_{(n+1)}O_{(2n+3)}^{2-} - 2e^- = (n+1)CO_2(g) + 0.5O_2\ (g)\ (n \geq 0) \quad (6)$$

In order to make the reactions progress at a reasonable rate, a cost-affordable anode with long-term stability is necessary. Although materials like Pt, Ir, SnO_2, $CaRuO_3$ and $Ni_{10}Cu_{11}Fe$ alloy have been used as the inert anodes in various molten salt systems,[22,35–37] a comprehensive analysis of inert anode selection in the Li_2CO_3–Na_2CO_3–K_2CO_3 molten eutectic is still absent. Thus, a series of anode materials including Ni, Fe, Cu, Pt, Ir, SnO_2 and $Ni_{10}Cu_{11}Fe$ alloy were investigated. In Fig. 4a, the anodic behaviors of Ni, Fe and Cu electrodes in the Li_2CO_3–Na_2CO_3–K_2CO_3 eutectic are presented. It is noted that, for the Ni and Fe electrodes, the anodic currents in the forward scans are much higher than those of the reverse scans. In contrast, the Cu working electrode does not show any noticeable current difference between the forward and reverse scans. The three electrodes were carefully examined after the anodic polarization scan and their appearances before and after measurement are compared in Fig. S5 in the ESI.† For the Ni and Fe electrodes, dissolution of metal can be observed, which explains the higher currents in the forward scan. In the case of the Cu electrode, a layer of black CuO formed, but the diameter of electrode did not change, indicating a better resistance to the chemical attack of the electrolyte. Compared with the copper oxide, the nickel oxide and iron oxide are believed to be more soluble in the Li_2CO_3–Na_2CO_3–K_2CO_3 eutectic, resulting in a quick corrosion of the metallic electrode.

Fig. 4b depicts the anodic polarization behaviors of Pt, Ir and SnO_2 electrodes in molten Li_2CO_3–Na_2CO_3–K_2CO_3 at 500 °C. As can be seen, all three electrodes present smooth profiles, and the currents of forward and reverse scans do not show obvious differences. The onset potentials of oxygen evolution of the three electrodes are all around 0.5 V *vs* Ag quasi reference,

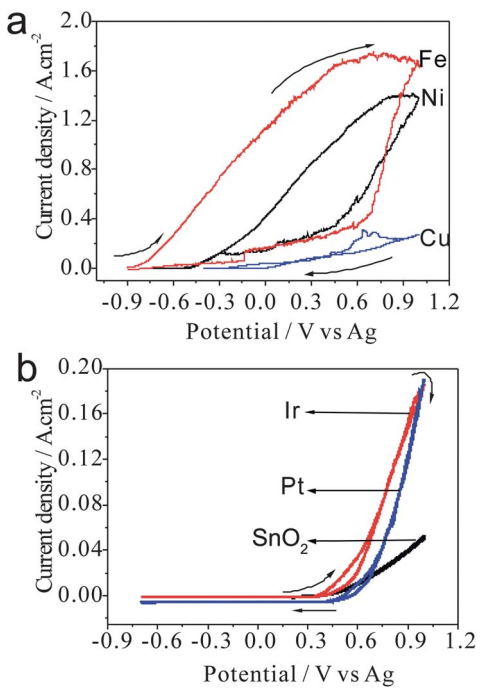

Fig. 4 (a) Polarization curves of the Ni, Fe, Cu electrodes and (b) Pt, Ir, SnO_2 electrodes in molten Li_2CO_3–Na_2CO_3–K_2CO_3 at 500 °C in the CO_2 atmosphere, scan rate: 5 mV s^{-1}.

meanwhile, Pt and Ir electrodes exhibit better catalytic performance than SnO_2 for oxygen evolution in this eutectic in terms of the slope of the polarization curve. However, considering that Pt and Ir are both costly noble metals, only the SnO_2 electrode was further tested using constant cell voltage electrolysis.

The appearances of the Ni anode, Ni10Cu11Fe alloy anode and SnO_2 anode (before and after constant voltage electrolysis) are given in Fig. 5a. It is not unexpected that the Ni anode was seriously corroded (corrosion rate was about 12 mm per day). After 2 hours of electrolysis, the residual corrosion product on the electrode, collected from the side close to the electrolyte–headspace interface, was identified as NiO (see XRD spectra in Fig. S6 in the ESI†). Ni10Cu11Fe alloy was proven to be a desirable anode for the Na_2CO_3–K_2CO_3 molten system in our previous research,[25] whereas its electrochemical stability in the Li_2CO_3–Na_2CO_3–K_2CO_3 eutectic is not acceptable since many corrosion pits were observed after 2 hours of electrolysis. Because ferric oxide has a relatively high solubility in molten Li_2CO_3,[38] the ferric oxide at the surface cannot form a dense layer to prevent the inner alloy from being attacked. Hence, pitting corrosion rather than uniform corrosion was observed on the Ni10Cu11Fe alloy anode. In contrast, the shape and appearance of the SnO_2 anode did not reveal obvious change even after 500 hours of electrolysis, and the change of electrode mass was less than 0.1%. This observation confirms that the SnO_2 anode is viable for long-term service in the molten Li–Na–K carbonate eutectic, which is crucial to the future scale-up of the MSCC-ET process.

When CO_2 gas was fed into the carbonate melt at 50 mL min^{-1}, the gas from the headspace of the reactor was analyzed using GC. As shown in Fig. 5b, no CO was detected in the gas, indicating carbon is the only product of cathodic reduction at the experimental temperature. This is in accord with previous research conducted by Licht *et al.* and Kaplan *et al.*[20,22] The N_2 and CO_2 concentrations in the headspace did not show any significant change, however, the peak assigned to O_2 showed a sharp rising during the electrolysis (O_2 content rose from 1.4 mol% to 13.5 mol% in the effluent gas), confirming the production of O_2 at the anode.

Current efficiency and energy consumption

Fig. 6a presents the current–time plots of the electrolysis under different cell voltages. At 2.8 V, the current was constantly low and only a thin carbon film was obtained after 2 hours of electrolysis. When the cell voltage was increased to 3.0 V, the increasing current *vs.* time indicates the expansion of the electrode surface due to the deposition of carbon. At 4.0 V cell voltage, the current increased up to approximately 1200 mA, indicating the electrochemical reactions were progressing vigorously. At 5.0 V, the current sharply increased within 5 minutes and then experienced a slow decrease. The decrease of current at the later stage of electrolysis is probably caused by the increasing IR drop when the deposited porous carbon was growing thicker. In terms of the mass of the

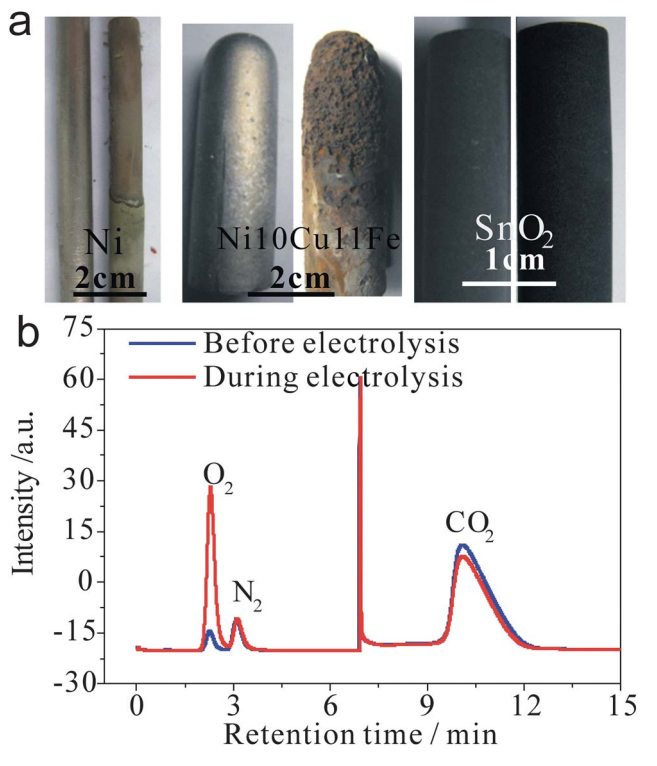

Fig. 5 (a) Digital photos of Ni, Ni10Cu11Fe and SnO_2 electrodes before and after serving as the anode under a constant cell voltage of 3.0 V in Li_2CO_3–Na_2CO_3–K_2CO_3 melts at 500 °C (2 hours for Ni and Ni10Cu11Fe anodes, more than 500 hours for SnO_2 anode) and (b) gas chromatograms of the outlet gas before and during electrolysis (1 hour, 4.5 V cell voltage) using the SnO_2 anode.

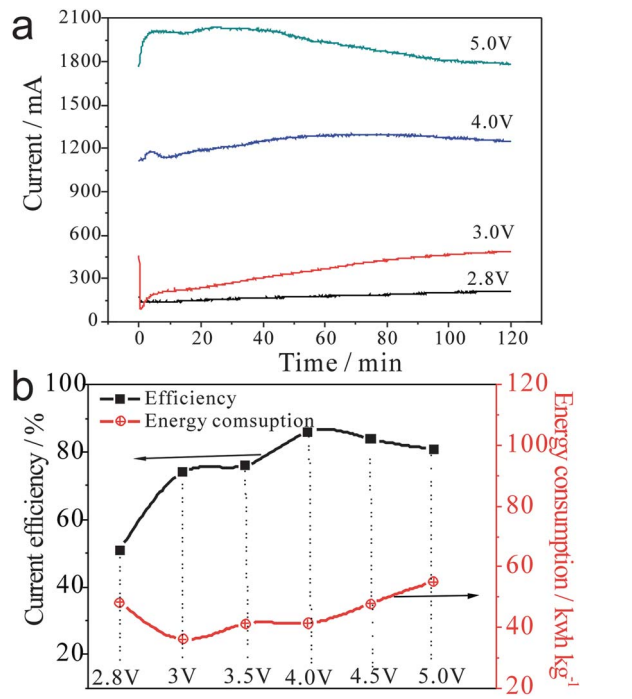

Fig. 6 Current–time plots of the electrolysis at the indicated cell voltages (a) and the plot of current efficiency and energy consumption with the electrolysis cell voltage (b).

obtained carbon, the current efficiency and energy consumption of electrolysis are calculated and given in Fig. 6b. As can be seen, the current efficiency increased with the cell voltage from 2.8 V to 4.0 V and then slightly decreased after 4.0 V, but the current efficiencies at cell voltages exceeding 2.8 V are all more than 70%. In contrast to the electrochemical reduction of CO_2 in aqueous solution or in RTILs,[12,14,39] the current efficiency presented in this molten salt system is obviously preferable. Considering that the current densities of the Ni cathode are more than 50 mA cm^{-2} (calculated from Fig. 6a, with respect to 12 cm^2 Ni cathode) when cell voltages are positive of 4 V, the electrochemical reactions apparently progressed at a pretty fast rate with high current efficiencies, which means the present technology can be engineered for a high flux transformation of CO_2. Likewise, the higher current efficiency also results in a relatively low energy consumption for carbon generation: the minimum energy consumption of 38 kW h kg^{-1} was obtained at 3 V, in other words, the conversion energy of CO_2 is 10.4 kW h kg^{-1}. The energy penalty of an electrolysis process is mostly dependent on the equilibrium potential of the rate-limiting reaction, the overpotentials of electrode reactions, and the IR drop of the electrolyte. The latter two factors can be further improved by optimizing the design of the electrolytic cell, such as using large surface area electrodes and shortening the distance between the anode and cathode. Therefore, it is expected that value-added capacitive carbon materials and oxygen gas can be produced by splitting CO_2 at more reasonable energy consumption.

Conclusions

The present study demonstrated an effective MSCC-ET process for the capture and electrochemical conversion of CO_2 in the molten Li_2CO_3–Na_2CO_3–K_2CO_3 in a cell fitted with cost-affordable electrodes. CO_2 gas was captured by the O^{2-} ions (or by lithium oxide) and electrochemically reduced into useful products with a high current efficiency. The porous carbon from the cathodic reaction exhibits a BET surface area excess of 414 m^2 g^{-1}, being advantageous for its use for capacitive and adsorbent materials. The SnO_2 anode is proven to be viable for long-term use in the Li_2CO_3–Na_2CO_3–K_2CO_3 eutectic. Compared with previously reported CCS processes, the MSCC-ET process has some unique characteristics favoring its large-scale application: working at the lower temperature of 500 °C; intrinsic ability to capture CO_2; use of affordable electrodes like a Ni cathode and a SnO_2 anode; capable of producing value-added carbon materials and oxygen; high flux transformation of CO_2 at reasonable current efficiency and thus expected lower energy consumption; amenable to combine with a renewable energy source like solar power. As a compact CO_2 capture and conversion process, the MSCC-ET can be applied at a large scale for the capture and utilization of the CO_2 effluent of industrial processes. In addition, it can be designed for exploring outer space, for example, recycling CO_2 and providing oxygen for people in the spacecraft using the carbonates from outer space.[40–42]

Acknowledgements

The authors thank the NSFC (Grant no. 20873093, 50934001, 51071112), MOE of China (NCET-08-0416) and the Fundamental Research Funds for Central Universities of China for financial support.

Notes and references

1 P. N. Pearson and M. R. Palmer, *Nature*, 2000, **406**, 695–699.
2 M. Pagani, Z. H. Liu, J. LaRiviere and A. C. Ravelo, *Nat. Geosci.*, 2010, **3**, 27–30.
3 P. Friedlingstein, P. Cox, R. Betts, L. Bopp, W. Von Bloh, V. Brovkin, P. Cadule, S. Doney, M. Eby, I. Fung, G. Bala, J. John, C. Jones, F. Joos, T. Kato, M. Kawamiya, W. Knorr, K. Lindsay, H. D. Matthews, T. Raddatz, P. Rayner, C. Reick, E. Roeckner, K. G. Schnitzler, R. Schnur, K. Strassmann, A. J. Weaver, C. Yoshikawa and N. Zeng, *J. Clim.*, 2006, **19**, 3337–3353.
4 H. Arakawa, M. Aresta, J. N. Armor, M. A. Barteau, E. J. Beckman, A. T. Bell, J. E. Bercaw, C. Creutz, E. Dinjus, D. A. Dixon, K. Domen, D. L. DuBois, J. Eckert, E. Fujita, D. H. Gibson, W. A. Goddard, D. W. Goodman, J. Keller, G. J. Kubas, H. H. Kung, J. E. Lyons, L. E. Manzer, T. J. Marks, K. Morokuma, K. M. Nicholas, R. Periana, L. Que, J. Rostrup-Nielson, W. M. H. Sachtler, L. D. Schmidt, A. Sen, G. A. Somorjai, P. C. Stair, B. R. Stults and W. Tumas, *Chem. Rev.*, 2001, **101**, 953–996.
5 P. G. Jessop, Y. Hsiao, T. Ikariya and R. Noyori, *J. Am. Chem. Soc.*, 1996, **118**, 344–355.
6 T. Sakakura, J. C. Choi and H. Yasuda, *Chem. Rev.*, 2007, **107**, 2365–2387.
7 R. Angamuthu, P. Byers, M. Lutz, A. L. Spek and E. Bouwman, *Science*, 2010, **327**, 313–315.
8 G. Centi and S. Perathoner, *Catal. Today*, 2009, **148**, 191–205.
9 M. Mikkelsen, M. Jorgensen and F. C. Krebs, *Energy Environ. Sci.*, 2010, **3**, 43–81.
10 A. A. Peterson, F. Abild-Pedersen, F. Studt, J. Rossmeisl and J. K. Norskov, *Energy Environ. Sci.*, 2010, **3**, 1311–1315.
11 M. Gattrell, N. Gupta and A. Co, *J. Electroanal. Chem.*, 2006, **594**, 1–19.
12 N. V. Rees and R. G. Compton, *Energy Environ. Sci.*, 2011, **4**, 403–408.
13 J. E. Bara, D. E. Camper, D. L. Gin and R. D. Noble, *Acc. Chem. Res.*, 2010, **43**, 152–159.
14 X. P. Zhang, X. C. Zhang, H. F. Dong, Z. J. Zhao, S. J. Zhang and Y. Huang, *Energy Environ. Sci.*, 2012, **5**, 6668–6681.
15 Z. Z. Yang, Y. N. Zhao and L. N. He, *RSC Adv.*, 2011, **1**, 545–567.
16 H. Kawamura and Y. Ito, *J. Appl. Electrochem.*, 2000, **30**, 571–574.
17 B. Kaplan, H. Groult, S. Komaba, N. Kumagai and F. Lantelme, *Chem. Lett.*, 2001, **7**, 714–715.
18 B. Kaplan, H. Groult, A. Barhoun, F. Lantelme, T. Nakajim, V. Gupta, S. Komab and N. Kumagai, *J. Electrochem. Soc.*, 2002, **149**, D72–D78.

19 K. Le Van, H. Groult, F. Lantelme, M. Dubois, D. Avignant, A. Tressaud, S. Komaba, N. Kumagai and S. Sigrist, *Electrochim. Acta*, 2009, **54**, 4566–4573.
20 V. Kaplan, E. Wachtel, K. Gartsman, Y. Feldman and I. Lubomirsky, *J. Electrochem. Soc.*, 2010, **157**, B552–B556.
21 J. Schneider, H. Jia, K. Kobiro, D. E. Cabelli, J. T. Muckerman and E. Fujita, *Energy Environ. Sci.*, 2012, **5**, 9502–9510.
22 S. Licht, B. H. Wang, S. Ghosh, H. Ayub, D. L. Jiang and J. Ganley, *J. Phys. Chem. Lett.*, 2010, **1**, 2363–2368.
23 N. J. Siambun, H. Mohamed, D. Hu, D. Jewell, Y. K. Beng and G. Z. Chen, *J. Electrochem. Soc.*, 2011, **158**, H1117–H1124.
24 V. Kaplan, E. Wachtel and I. Lubomirsky, *J. Electrochem. Soc.*, 2012, **159**, E159–E161.
25 H. Y. Yin, D. Y. Tang, H. Zhu, Y. Zhang and D. H. Wang, *Electrochem. Commun.*, 2011, **13**, 1521–1524.
26 S. Viamajala, B. M. Peyton, W. A. Apel and J. N. Petersen, *Biotechnol. Bioeng.*, 2002, **78**, 770–778.
27 P. Claes, D. Moyaux and D. Peeters, *Eur. J. Inorg. Chem.*, 1999, 583–588.
28 P. Claes, D. Moyaux and D. Peeters, *Eur. J. Inorg. Chem.*, 1999, 589–592.
29 V. Kaplan, E. Wachtel and I. Lubomirsky, *J. Chem. Thermodyn.*, 2011, **43**, 1623–1627.
30 *Raman scattering in carbon materials*, ed. M. S. Dresselhaus, G. Dresselhaus, M. A. Pimenta and P. C. Ehlund, Blackwell Science, New York, 1999.
31 Y. R. Nian and H. S. Teng, *J. Electrochem. Soc.*, 2002, **149**, A1008–A1014.
32 M. Inagaki, H. Konno and O. Tanaike, *J. Power Sources*, 2010, **195**, 7880–7903.
33 D. Mohan and C. U. Pittman, *J. Hazard. Mater.*, 2006, **137**, 762–811.
34 A. Kumar, D. Suman, B. Chiranjib and D. Siddhartha, *Chem. Eng. J.*, 2011, **173**, 135–143.
35 D. H. Wang, A. J. Gmitter and D. R. Sadoway, *J. Electrochem. Soc.*, 2011, **158**, E51–E54.
36 H. Y. Yin, L. L. Gao, H. Zhu, X. H. Mao, F. X. Gan and D. H. Wang, *Electrochim. Acta*, 2011, **56**, 3296–3302.
37 S. Q. Jiao and D. J. Fray, *Metall. Mater. Trans. B*, 2010, **41**, 74–79.
38 S. Licht and B. H. Wang, *Chem. Commun.*, 2010, **46**, 7004–7006.
39 Y. G. Zhang and J. Y. G. Chan, *Energy Environ. Sci.*, 2010, **3**, 408–417.
40 I. G. Mitrofanov, M. T. Zuber, M. L. Litvak, W. V. Boynton, D. E. Smith, D. Drake, D. Hamara, A. S. Kozyrev, A. B. Sanin, C. Shinohara, R. S. Saunders and V. Tretyakov, *Science*, 2003, **300**, 2081–2084.
41 W. V. Boynton, D. W. Ming, S. P. Kounaves, S. M. M. Young, R. E. Arvidson, M. H. Hecht, J. Hoffman, P. B. Niles, D. K. Hamara, R. C. Quinn, P. H. Smith, B. Sutter, D. C. Catling and R. V. Morris, *Science*, 2009, **325**, 61–64.
42 P. B. Niles, W. V. Boynton, J. H. Hoffman, D. W. Ming and D. Hamara, *Science*, 2010, **329**, 1334–1337.